Journal of The Electrochemical Society, **150** (11) A1432-A1439 (2003)
0013-4651/2003/150(11)/A1432/8/$7.00 © The Electrochemical Society, Inc.

Quasi-3D Modeling of Water Transport in Polymer Electrolyte Fuel Cells

A. A. Kulikovsky[a]

Research Center "Jülich", Institute for Materials and Processes in Energy Systems (IWV-3), D-52425 Jülich, Germany

Model of water transport in a membrane electrode assembly of a polymer electrolyte fuel cell (PEFC) is developed. The model takes into account nonlinear diffusion of liquid water in the membrane. It is shown that nonlinearity leads to the formation of closely located dry and wet regions in the membrane. The model is incorporated into our quasi-3D model of a PEFC and recent experiments of Büchi and Scherer are simulated. The model qualitatively reproduces measured membrane resistance and the mean profile of water content across the membrane. Calculated two-dimensional distribution of water in the cell cross section is discussed.
 [DOI: 10.1149/1.1611489]

Manuscript submitted February 27, 2003; revised manuscript received April 29, 2003. Available electronically September 16, 2003.

Membranes play a vital role in polymer electrolyte fuel cells (PEFCs). The membrane has to prevent mixing of feed gases and provide good transport of protons from the anode to the cathode.

State-of-the art polymer electrolytes (such as Nafion) have noticeable ionic conductivity only in a wet state. Under sufficient hydration the molecules of a polymer backbone form water-filled microchannels with SO_3^- groups attached to their walls. In the external electric field protons are transported in these microchannels either due to hopping between adjacent water molecules (Grottus mechanism) or due to formation and drift of H_3O^+ molecules (vehicle mechanism). The structure of the membrane (number of conducting channels, their mean radius, and form) depends on water content λ, the number of water molecules per SO_3^- group. Structural changes lead to strong dependence of membrane transport parameters (including proton conductivity) on λ. This is an important issue in overall cell performance; water transport in the membrane is essentially nonlinear.

The first 1D model of a PEFC which took into account water transport in the membrane was developed by Springer *et al.*[1] They assumed a diffusion mechanism of transport and used a measured dependence of the diffusion coefficient of water in membrane $D_{wl}(\lambda)$. However, below $\lambda = 2$ no data on D_{wl} were presented.

One year later, Bernardi and Verbrugge[2] assumed that water is transported through the membrane due to pressure gradient and used constant hydraulic permeability in the expression for water flux.[b] Since that time the nature of the driving force for water transport (pressure gradient or concentration gradient) has been discussed in literature.

In multidimensional modeling of PEFC water transport in membrane is usually described in a simplified manner. The first quasi-2D, along-the-channel model of a PEFC was developed by Fuller and Newman[5] under the assumption of constant D_{wl}. Recently Futerko and Hsing[6,7] took into account the dependence $D_{wl}(\lambda)$. Their model, however, does not resolve catalyst layers and hence ignores the influence of spatial nonuniformity of λ on catalyst layer performance.

Um *et al.*[8] assumed that D_{wl} is constant, Nguyen and White,[9] Yi and Nguyen,[10] and Thirumalai and White[11] employed assumptions of constant pressure gradient and constant gradient of water concentration across the membrane. Dannenberg *et al.*[12] and van Bussel *et al.*[13] took into account the dependencies of diffusion and drag coefficients on λ, however, it is unclear whether the equations of water balance were solved or water content was estimated in a simplified manner in these works. Natarajan and Nguyen[14] developed a two-phase model of water transport on the cathode side of membrane electrode assembly (MEA). However, their model does not resolve the catalyst layer and water transport in the membrane is not considered. In a fully 3D model of PEFC (Dutta *et al.*,[15] Shimpalee and Dutta[16]) constant gradient of water concentration across the membrane is assumed. In our across-the-channel model[17] and quasi-3D model[18] the membrane is assumed to be fully hydrated. Recently Janssen[19] developed a detailed model of water transport in PEFCs. The flux of water in the membrane is taken to be proportional to the gradient of chemical potential; the respective coefficient in the expression for the flux (membrane permeability) is assumed constant. Hence, nonlinear effects are out of the scope of this model.

Recent measurements[13] have shown that D_{wl} rapidly decreases as $\lambda \to 0$ (see Appendix). The aim of this work is to study nonlinear effects in water transport through the membrane in a PEFC environment. To demonstrate qualitatively the role of nonlinearity, we first solve a simple 1D model equation. The solution shows that a region with a very high gradient of water content may arise in a membrane. These thin regions separate dry and well-humidified domains. The model of water transport then is incorporated into our quasi-3D model of a PEFC[18] and recent experiments of Büchi and Scherer[20,21] are simulated. Comparison with experiment is presented and the effect of 2D nonuniformity of water distribution on cell performance is discussed.

The Model

Basic assumptions.—The kinetics of channel formation in Nafion membranes upon water uptake and even geometry of channels is not well understood. The situation is complicated by the fact that the structure of the membrane depends on the method of material pretreatment. Exposure of the membrane under different hydration and thermal conditions leads to formation of different pore structures and thus to different macroscopic properties of the membrane. Extensive review of these issues was published by Gottesfeld and Zawodzinski.[22]

The microscopic mechanisms of water transport in membranes are also questionable.[22] Under high water content mobility of water molecules within the pore corresponds to mobility in bulk water environment. However, mobility of water rapidly decreases with λ. This suggests that under high water content the mean radius of water-filled channels is large and the transport of polar water molecules is not affected by side SO_3^- groups. When channel radius decreases, the transport of water is hindered by the electrical field of side charges.

In PEFC modeling detailed account of microscopic mechanisms of water transport in polymer electrolyte is redundant. This is a task for physical modeling of membranes. PEFC models consider membranes as a homogeneous media with given dependencies of macroscopic transport parameters (diffusion coefficient of water, proton mobility, etc.) on water content.

[a] On leave from Moscow State University, Research Computing Center, 119992 Moscow, Russia.

[b] Their model was recently modified and successfully applied to description of PEFC performance curves by Murgia *et al.*[3] and Pisani *et al.*[4]

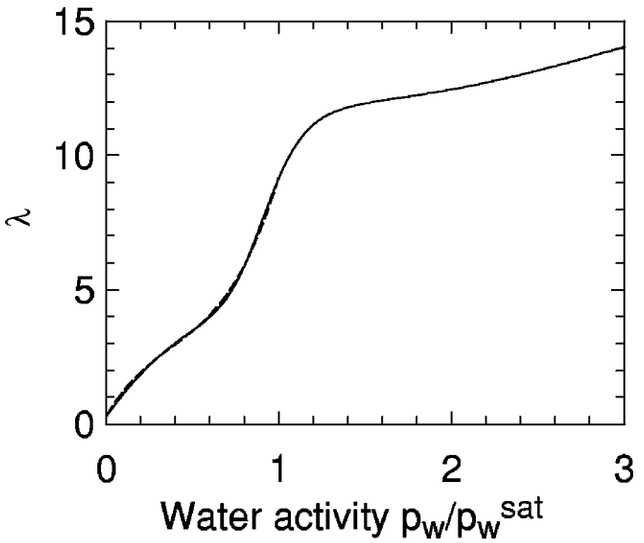

Figure 1. Water uptake of Nafion membrane, equilibrated with water vapor: (— — —) fit of experimental data,[23] (——) the curve used in the simulations.

In the catalyst layers water is transported both in liquid and vapor form. Polymer electrolyte provides the pathways for liquid water, and vapor is transported through the voids. Backing layers contain no electrolyte and water is transported through these layers only in gas phase.

Our model is based on the following assumptions: (*i*) formation of liquid water droplets in voids is neglected, and (*ii*) in the catalyst layers, liquid water in membrane phase is equilibrated with water vapor in voids.

We, therefore, assume that water in the cell exists in two forms: vapor fills voids of the porous (backing and catalyst) layers and liquid water exists in bulk membrane and in the membrane phase of the catalyst layer. In the catalyst layers, liquid water in the membrane phase is equilibrated with the water vapor in voids.

The fundamental characteristic of the membrane in our model is the water sorption isotherm, which gives the water content of the membrane, equilibrated with water vapor of a given activity a. Figure 1 shows the water sorption curve used in our simulations. Below $a = 1$ the curve in Fig. 1 fits the experimental data[23] for Nafion at 80°C. The model ignores liquid droplets in voids. In the following,[1] the effect of condensation is taken into account approximately, assuming that water vapor activity can exceed 1. For that reason the curve $\lambda(a)$ is extrapolated to $a = 3$, as shown in Fig. 1. The maximal water uptake of membrane, equilibrated with ''supersaturated'' vapor, is 14. The latter value is a model parameter (see Discussion section).

Water flux in different regions.—Recent experiments[19] have shown that pressure gradient has a minor affect on water transport in the membrane. In the membrane water flux $\mathbf{N}_w$ is assumed to be

$$\mathbf{N}^w = -D_{wl}(\lambda)\nabla c_{wl} + n^d\frac{j}{F} \qquad [1]$$

where c_{wl} and D_{wl} is concentration and diffusion coefficient of liquid water in membrane, and $n^d(\lambda)$ is drag coefficient.

The catalyst layer contains electrolyte (membrane) phase and voids. We assume that in small pores water vapor is transported due to Knudsen diffusion. Three mechanisms, hence, contribute to water transport in catalyst layers: diffusion and drag in the membrane phase and Knudsen diffusion in voids. Flux in the membrane phase is Eq. 1, multiplied by correction factor ε, which accounts for amount of electrolyte in the active layer. This gives

$$\mathbf{N}_w = -D_w^K\nabla c_w + \varepsilon\left(-D_{wl}(\lambda)\nabla c_{wl} + n^d\frac{\mathbf{j}}{F}\right) \qquad [2]$$

where c_w is molar concentration of vapor and

$$D_w^K = \psi\bar{r}\sqrt{\frac{8RT}{\pi M_w}} \qquad [3]$$

is the Knudsen diffusion coefficient of water vapor in voids. Here ψ is a correction factor, $\bar{r}$ is a mean pore radius, and the square root is a mean thermal velocity of water molecules. To a first approximation ε can be taken equal to the volume fraction of the membrane phase.

In the catalyst layers c_{wl} in membrane phase is related to vapor concentration c_w in voids via the sorption isotherm $\Lambda(a)$

$$\lambda \equiv \frac{c_{wl}}{c_{H^+}} = \Lambda(a) = \Lambda\left(\frac{c_w}{c_w^{sat}}\right) \qquad [4]$$

where $a = c_w/c_w^{sat}$ is water activity and c_w^{sat} is a molar concentration of saturated water vapor. With Eq. 4 we can write

$$-D_{wl}\nabla c_{wl} = -D_{wl}\frac{c_{H^+}}{c_w^{sat}}\frac{\partial\Lambda}{\partial a}\nabla c_w = -D_w\nabla c_w \qquad [5]$$

where

$$D_w = D_{wl}\frac{c_{H^+}}{c_w^{sat}}\frac{\partial\Lambda}{\partial a} \qquad [6]$$

is the diffusion coefficient of equivalent water vapor in the membrane phase.

Water concentration exhibits discontinuity at the surface of the membrane: in the membrane water is in liquid state, whereas in the voids of the catalyst layer water is in vapor form. This discontinuity is treated explicitly in the problem of water transport in bulk membrane (see Eq. 11). In the catalyst layer, membrane phase forms a tortuous structure and the use of boundary condition Eq. 11 is not possible. However, the ratio of the surface of membrane phase to its volume in the active layer is many orders of magnitude larger than this ratio for bulk membrane. This justifies the use of Eq. 4 and 6 in the active layer.

Finally, in the catalyst layers we have

$$\mathbf{N}_w = -D_w^K\nabla c_w + \varepsilon\left(-D_w(\lambda)\nabla c_w + n^d\frac{\mathbf{j}}{F}\right) \qquad [7]$$

The backing layers contain no membrane phase and mean pore radius in these layers is much larger than the mean-free path of molecules. Binary (molecular) diffusion is hence the main mechanism of gas transport in backing layers.

Binary diffusion is usually described by Stefan-Maxwell formulas, which relate interdiffusion fluxes in a gas mixture.[24] However, handling the equations which follow from Stefan-Maxwell formulas in multidimensional modeling is a difficult and computationally expensive task.[25] Our experience shows that the use of a simple Fick's formula with the effective diffusion coefficient D_w^b leads to much faster algorithms and gives practically the same result. This conclusion is confirmed by recent numerical experiments by Stockie *et al.*[26]

In backing layers the flux of water, therefore, is assumed to be

$$\mathbf{N}_w = -D_w^b\nabla c_w \qquad [8]$$

where D_w^b is determined by

$$\frac{\zeta^{1.5}}{D_w^b} = \sum_j\frac{\xi_j}{D_{wj}}$$

Table I. The flux of water in different regions. The third row shows the respective diffusion coefficients.

	Backing layer	Catalyst layer	Membrane
$\mathbf{N}_w$	$-D_w^b \nabla c_w$	$-D_w^K \nabla c_w + \varepsilon\left(-D_{wl}\nabla c_w + n^d \frac{\mathbf{j}}{F}\right)$	$-D_{wl}(\lambda)\nabla c_{wl} + n^d \frac{j}{F}$
D/cm^2 s^{-1}	$D_w^b \simeq 10^{-1}$-10^{-2}	$D_w^K \simeq 10^{-2}$-10^{-3}, $D_w = 0$-10^{-2}	$D_{wl} \simeq 0$ to 10^{-5}

Here ζ is backing layer porosity, ξ_j is molar fraction of jth component, and D_{wj} is binary diffusion coefficient of water vapor in the mixture with j-th species.[24]

Table I lists the expressions for fluxes and respective diffusion coefficients in all layers.

Mass conservation equations.—In the cathode catalyst layer water is produced in electrochemical reaction; in all other domains there are no sinks and sources of water. The mass conservation equation of water has, therefore, the form

$$\nabla \cdot \mathbf{N}_w = \begin{cases} \frac{S_w}{nF} Q, & \text{in the cathode catalyst layer} \\ 0, & \text{otherwise} \end{cases} \quad [9]$$

where $\mathbf{N}_w$ is given by Eq. 1, 7, and 8 in the respective layer.

Conditions at the membrane-catalyst layer interface.—Because water is transported through the membrane in liquid form, the membrane surface is impermeable for water vapor. Diffusion flux of water vapor on both sides of the membrane is hence zero

$$\left.\frac{\partial c_w}{\partial x}\right|_{x=x_{a,c}} = 0 \quad [10]$$

where $x_{a,c}$ is the coordinate of the membrane/catalyst layer interface.

Water content of the membrane surface is determined by local vapor concentration via a sorption isotherm. Thus, on both sides of the membrane we have

$$c_{wl}|_{x=x_{a,c}} = c_{H^+}\Lambda\left(\frac{c_w|_{x=x_{a,c}}}{c_w^{sat}}\right) \quad [11]$$

where $c_w|_{x=x_{a,c}}$ is vapor concentration at the membrane surface.

Equation 9 provides the overall mass balance of water in the cell. Equations 10 and 11 mean that only electro-osmotic flux through the membrane surface is allowed, *i.e.*, we neglect "back" transport of liquid water from the membrane to the anode catalyst layer. Physically, already at moderate current density electro-osmotic flux exceeds diffusion flux. Besides, the membrane binds water; it is a "sponge" which can bind up to 14 water molecules per SO_3^- group and back-diffusion of water from such a sponge is hindered. One may expect "back" flux of liquid water to the anode catalyst layer due to the capillary effects. This process, however, is out of the scope of our model.

Numerical procedure.—The distribution of water in the MEA is determined in two steps. First, solving Eq. 9 with the fluxes (Eq. 8 and 7) and boundary conditions (Eq. 10) we obtain water vapor concentration in the backing and catalyst layers on both sides of the cell. Then the concentration of liquid water at the surfaces of the membrane is calculated with Eq. 11 and the problem in the bulk membrane is solved (Eq. 9 and 1).

The flux (Eq. 1) may induce numerical instability. If current is large, the electro-osmotic term in Eq. 1 dominates the diffusion term. The second derivative in the equation $\nabla \cdot \mathbf{N}_w = 0$ then disappears and the convergence of iterations fails.

To work around the problem the drag term can be transformed as follows. If n^d is constant, the electro-osmotic term in Eq. 1 can be omitted, since in the membrane $\nabla \cdot \mathbf{j} = 0$. The concentration of liquid water then is determined by the numerically stable equation

$$\nabla \cdot (D_{wl}\nabla c_{wl}) = 0 \quad [12]$$

If n^d is constant ($n^d = n_0^d$) over a certain range of λ (Fig. 2), stability of numerical calculations improves if one replaces n^d with $n^d - n_0^d$ in Eq. 1. If $n^d(\lambda)$ is not constant and the loss of convergence occurs, the electro-osmotic term should be calculated on a previous iteration step.

Modification of the quasi-3D model of PEFCs.—The model of water transport was incorporated into our quasi-3D (Q3D) model of PEFC.[18] In the previous version of the Q3D model it was assumed that membrane conductivity σ is constant. Since σ now varies with water content, the proton current conservation equation takes the form

$$\nabla \cdot [\sigma(\lambda)\nabla\varphi] = \begin{cases} -Q_a, & \text{in the anode catalyst layer} \\ 0, & \text{in the membrane} \\ Q_c, & \text{in the cathode catalyst layer} \end{cases} \quad [13]$$

where Q_a and Q_c are non-negative rates of protons production/consumption in the anode and the cathode catalyst layers, respectively, and φ is the potential of the membrane phase. Here $\sigma(\lambda)$ is determined on each iteration step using the fit given in the Appendix.

Membrane resistance.—Simulation enables us to determine the overall voltage loss δV in the bulk membrane and in the catalyst layers. This loss is calculated using the relation

$$I\delta V = \int_P \mathbf{j}\mathbf{E} d^3r = \int_P \sigma(\nabla\varphi)^2 d^3r \quad [14]$$

where I is total current produced by the fuel cell, $\mathbf{j} = -\sigma\nabla\varphi$ is proton current density, and $\mathbf{E} = -\nabla\varphi$ is electric field strength in the membrane phase. Integration in Eq. 14 is performed over the volume P of the membrane and the catalyst layers. Physically, Eq. 14 equates two expressions for total electrical power dissipated in the membrane phase. Membrane resistance (Ω cm^2) then is

$$R = \frac{\delta V}{\overline{j}} \quad [15]$$

where $\overline{j}$ is mean current density in the cell.

In the one-dimensional case, when current flows only across the membrane, one can calculate R simply as

$$R = \int_0^d \frac{dx}{\sigma(x)} \quad [16]$$

where d is overall thickness of membrane and catalyst layers. However, in the two-dimensional case proton current has arbitrary direction in membrane and Eq. 16 is no longer valid. Equation 14 (known in electrodynamics as Sato's theorem[27]) provides a rigorous way for δV calculation.

1D model problem.—If D_{wl} vanishes with c_{wl}, a nontrivial distribution of water in the membrane may arise when dry and wet

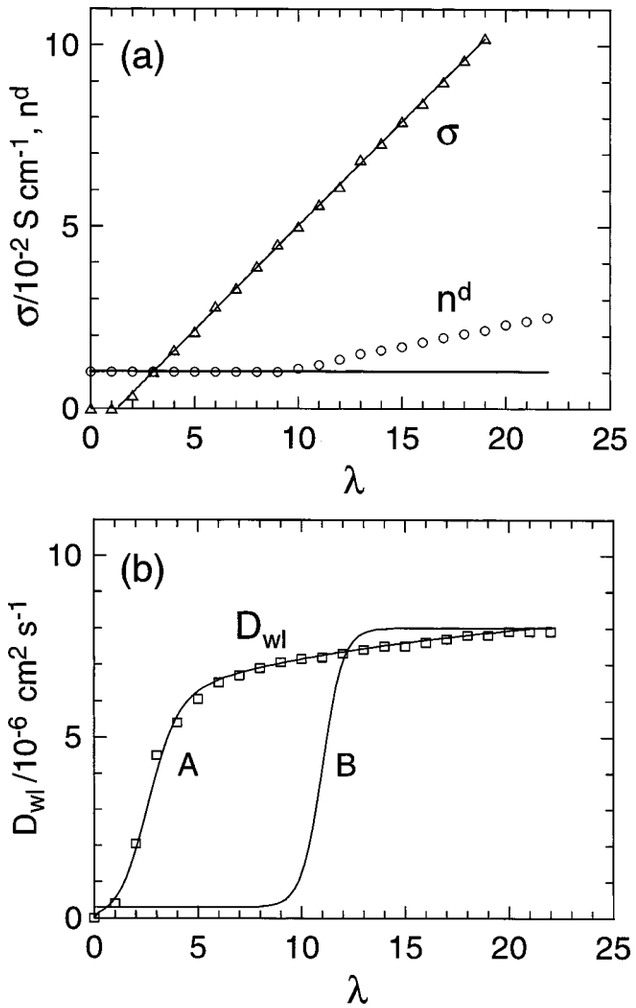

Figure 2. (a) Electro-osmotic drag coefficient n^d and membrane conductivity σ, (b) diffusion coefficient of water in membrane D_{wl}. (△, ○, □) Experimental data (Ref. 13) and (——) the curves used in the simulation. Curve A fits experimental data (Ref. 13), curve B is the model function (Eq. 20).

regions appear to be located close to each other. To illustrate this effect we consider a 1D model problem of water transport in an artificial membrane, in which diffusion and drag coefficients are proportional to the square of water concentration

$$\frac{\partial}{\partial x}\left(-c^2\frac{\partial c}{\partial x}+c^2\right)=0,\ c(1)=1,\ \left.\frac{\partial c}{\partial x}\right|_{x=1}=2 \qquad [17]$$

Here x is dimensionless distance, $x = 1$ is located at the membrane/cathode catalyst layer interface, and c is dimensionless water concentration, normalized to those at $x = 1$ (Fig. 3).

For simplicity we fix the concentration and water flux on the cathode side of the membrane (at $x = 1$). Equation 17 describes the situation when electro-osmotic and back-diffusion fluxes have opposite directions. The equation says that the total flux of water (expression in brackets on the left side) is constant. The solution to this equation is discussed in the next section.

Results

1D model problem.—Equation 17 is a 1D prototype of a general steady-state nonlinear convection-diffusion equation, Eq. 9 and 1. Equation 17 has the analytical solution $x(c)$. Apart from the physical effect, which is discussed below, this solution was used to check

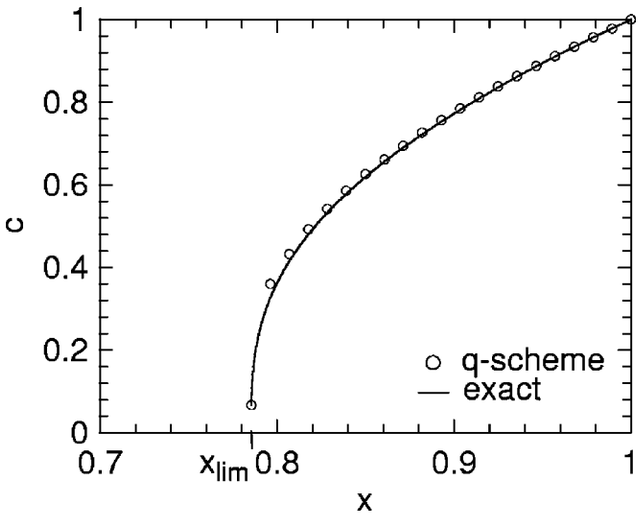

Figure 3. Water profile across the artificial membrane (solution to model equation, Eq. 17): (——) exact solution and (○) numerical solution with the *q*-scheme.

the quality of the numerical algorithm, developed specially for solution of Eq. 9 and 1 (*q*-scheme [28]). Figure 3 displays the exact and numerical solutions of Eq. 17.

Equation 17 states that water flux is constant along x and equals that flux prescribed by the boundary condition at $x = 1$. The flux of water in Eq. 17 consists of diffusion and drag components; the boundary condition at $x = 1$ hence corresponds to a certain proton current through the membrane.

The solution to Eq. 17 is shown in Fig. 3. It shows that water concentration c decreases as one moves from the cathode side of the membrane to the anode side. The diffusion coefficient (c^2 in Eq. 17) vanishes with c. The gradient of water concentration increases as x approaches x_{lim} in order to support the given water flux. At $x = x_{lim}$ this (finite) flux is a product of infinite gradient and zero water concentration. $1 - x_{lim}$ is hence a limiting thickness of membrane, which is able to support given current.

Appearance of infinite gradient of water concentration suggests that in real membranes the domains of high and low water content may be located very close to each other. A thin layer with a very high gradient of water content then separates these domains.

Note that a qualitatively similar solution with infinite gradient of c has the problem

$$\frac{\partial}{\partial x}\left(-c\frac{\partial c}{\partial x}+c\right)=0,\ c(1)=1,\ \left.\frac{\partial c}{\partial x}\right|_{x=1}=2$$

in which diffusion and drag coefficients are proportional to the first power of c.[28] Hence, the effect is due to the diffusion coefficient vanishing with c regardless of the exact dependence on c.

Simulation of Büchi and Scherer experiment.—Büchi and Scherer[21] reported results of *in situ* local measurements of membrane resistance in working fuel cells. To verify the model we performed simulation of PEFCs for their experimental conditions (Table II, "type 1" cell[20]).

The cell cross section[21] consists of a number of identical elements. The sketch of a single element is shown in Fig. 4. The two elements were simulated.

In the experiment a mean water profile across the membrane is measured. Our simulations give 2D distribution of water concentration in a cell cross section (Fig. 4). For comparison the mean power-weighed profile $\bar{\lambda}(x)$ was calculated according to

Table II. Conditions and parameters for simulation of Büchi and Scherer experiments.[20,28]

	Anode side	Cathode side
Cell temperature, C	60	60
Gas pressure, atm	3	3
Flow stoichiometry	1.5	1.5
Oxygen molar fraction		0.844
Water vapor molar fraction	0.156	0.156
Hydrogen molar fraction	0.844	
Transfer coefficient, α	0.5	1.0
Reaction order, γ	1	1
Volume fraction of electrolyte in the catalyst layers, ε	0.1	0.1
Correction factor ψ in Eq. 3	0.1	0.1
Mean pore radius $\bar{r}$ in Eq. 3, cm	10^{-6}	10^{-6}
Baking layer porosity, ζ	0.4	0.4
Carbon phase conductivity, Ω^{-1} cm^{-1}	40	
Catalyst layer thickness, μm	50	
Backing layer thickness, μm	300	
Membrane thickness, μm	200	
Channel width, cm	0.1	
Channel height, cm	0.2	
Current collector rib width, cm	0.15	

$$\bar{\lambda}(x) = \int_0^H \lambda(x,y)W(y)dy \qquad [18]$$

where the weighing function

$$W(y) = \frac{1}{I\delta V}\int_0^d \sigma(x,y)E^2(x,y)dx \qquad [19]$$

represents a fraction of electrical power, generated between the planes $y - dy/2$ and $y + dy/2$. Here δV is voltage loss in the membrane, given by Eq. 14, and H and d are shown in Fig. 4.

The function $W(y)$ obeys the relation

$$\int_0^H W(y)dy = 1$$

Physically, weighing Eq. 18 means that larger contribution to the mean water profile provides the regions with larger dissipated electrical power.

The diffusion coefficient of liquid water in membrane D_{wl} was taken from Ref. 13. The data[13] were fitted with the expression A-1 (see Appendix and curve A in Fig. 2b).

The mean profiles of water concentration are shown in Fig. 5 along with the measurements.[21] With the diffusion coefficient (curve A, Fig. 2b), the model predicts almost linear drop of $\bar{\lambda}$ across the membrane for all mean current densities (Fig. 5a). The reason is slow variation of diffusion coefficient with λ in the range $\lambda > 5$ (curve A in Fig. 2b). With D_{wl} (curve A, Fig. 2b), water content in membrane varies linearly as soon as $\lambda > 5$ on the anode side. The feature of experimental points, rapid fall of $\bar{\lambda}$ toward the anode, (Fig. 5) is not reproduced with this D_{wl}.

The experimental points in Fig. 5 suggest that D_{wl} rapidly changes at $\lambda \simeq 10$. To verify this idea we took the diffusion coefficient in the form

$$D_{wl} = D_{wl}^0 + (D_{wl}^1 - D_{wl}^0)\frac{1}{2}\left(1 + \tanh\left(\frac{\lambda - \lambda_0}{\Delta}\right)\right) \qquad [20]$$

(curve B in Fig. 2b). λ_0 determines the position of the transition region, where D_{wl} changes from small to large value, Δ is the width of this region.

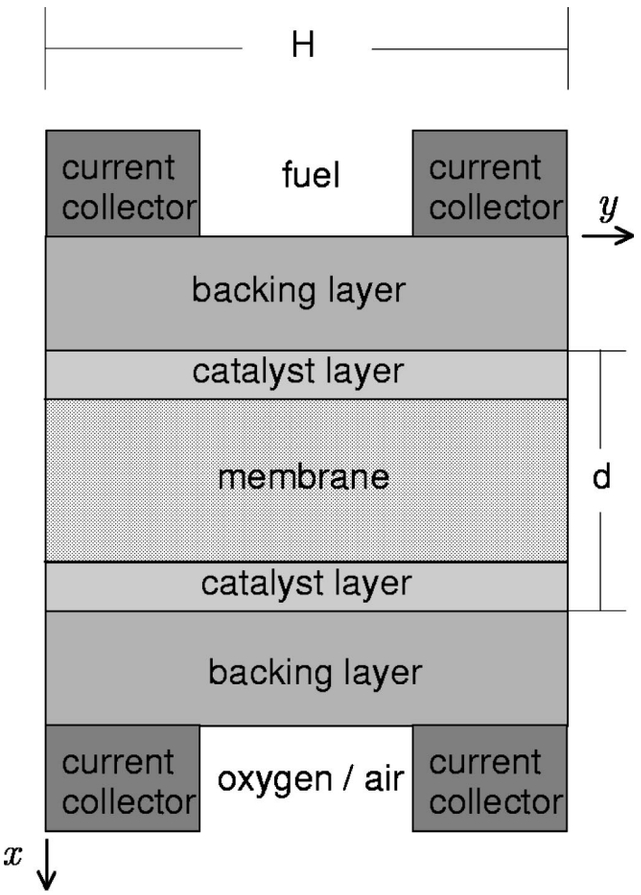

Figure 4. Geometry of the element of the cell cross section.

The result of the simulation with $\lambda_0 = 11$, $\Delta = 1$, $D_{wl}^0 = 3 \times 10^{-7}$ cm^2 s^{-1}, $D_{wl}^1 = 8 \times 10^{-6}$ cm^2 s^{-1} (curve B in Fig. 2b) is shown in Fig. 5b. With this D_{wl} the model qualitatively reproduces the profile of water content across the membrane and gives quite reasonable dependence of membrane resistance on $\bar{j}$ (Fig. 6). Note that the simulation with experimental D_{wl} (curve A, Fig. 2b) gives higher membrane resistance and worsens the shape of the curve $R(\bar{j})$ (Fig. 6).

"Noise" on the curves in Fig. 6 presumably is induced by the negative differential resistance (R decreases with $\bar{j}$), which leads to oscillations in membrane voltage loss. Physically, if R decreases with the growth of $\bar{j}$, two maps of water content correspond to the same mean current and both states of membrane presumably are unstable. The effect requires further investigation.

Figure 7 shows the maps of water content in the MEA cross section for two D_{wl} (curves A and B in Fig. 2b). In both cases water distribution in the MEA is very nonuniform. In front of the feed channels λ is almost constant across the cell. Channels impose "boundary conditions" for water concentration, which is the same on both sides. On the cathode side water is accumulated in front of the current collector rib, whereas on the other side the anode catalyst layer is dried out by electro-osmosis. In front of the ribs a high gradient of water content across the membrane arises (Fig. 8), which confirms qualitative prediction of a model equation, Eq. 17. Figure 7 and 8 clearly show that the growth of membrane resistance with current is caused by drying of the anode side by electro-osmosis, which occurs in front of the current collectors.

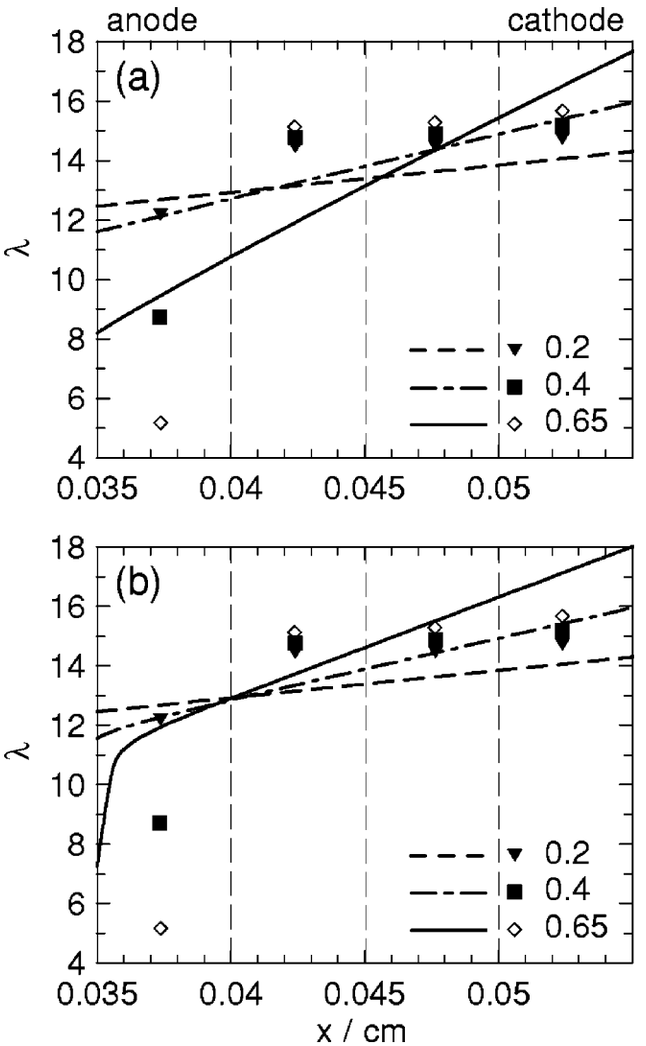

Figure 5. Profiles of water content across the membrane for indicated mean current densities in the cell (A cm^{-2}): (▼, ■, ◇) experimental data,[21] (lines) results of the simulation, (a) with experimental D_{wl} (curve A in Fig. 2b), and (b) with model D_{wl} (curve B in Fig. 2b).

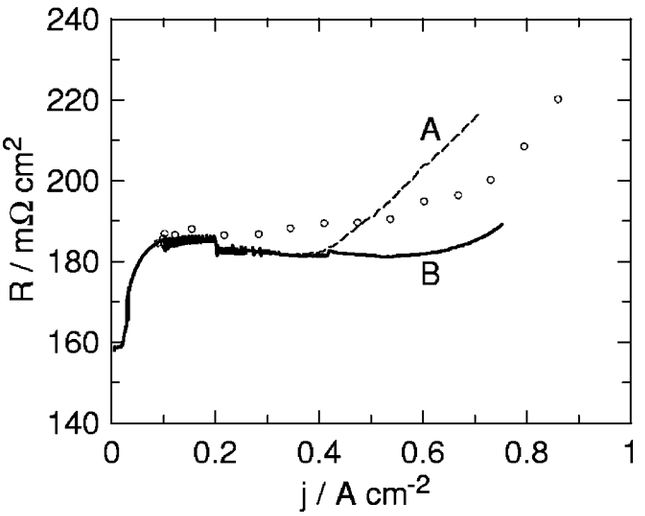

Figure 6. Membrane resistance: (A) simulation with the experimental diffusion coefficient D_{wl} (curve A in Fig. 2b), (B) simulation with the model D_{wl} (curve B in Fig. 2b), and (○) experimental data.[20]

Discussion

The diffusion coefficient of water in dry membranes is poorly known. To our knowledge, the results described in Ref. 13 are the only set of membrane transport parameters measured in working fuel cell environment available in the literature. Unfortunately, the details of the measurements[13] were not published.

Qualitatively, the data[13] displays an important feature of the membrane: below certain λ values the diffusion coefficient D_{wl} rapidly drops. A simple 1D model shows that such a nonlinearity may lead to very high gradients of water content in the membrane. Comparison of experiments[21] and 2D simulations qualitatively confirms this effect: in front of the current collector ribs a large gradient of λ arises.

Usually it is assumed that back-diffusion of water in a membrane partially compensates the drying of the anode side. If, however, D_{wl} vanishes with λ, back-diffusion is unable to supply the anode side with water. The model shows that the growth of membrane resistance with current, demonstrated in experiments of Büchi and Scherer, is caused by this nonlinear drying of the anode side. In that case the only way to support the required level of hydration of the anode catalyst layer is to supply additional water to the anode feed channel. In other words, once dried, the membrane cannot be returned to hydrated state by diffusion. This can only be done by changing the ''boundary condition'' in the anode channel.

One can reach a better fit of experimental curves $\overline{\lambda}(x)$ and $R(\overline{j})$ by varying the shape of the water sorption isotherm Λ above $a = 1$ (Fig. 1). Figure 5 suggests that $\Lambda(a > 1)$ is somewhat overestimated. This overestimates λ on the cathode side of the membrane (Fig. 5) and hence lowers the resistivity (Fig. 6).

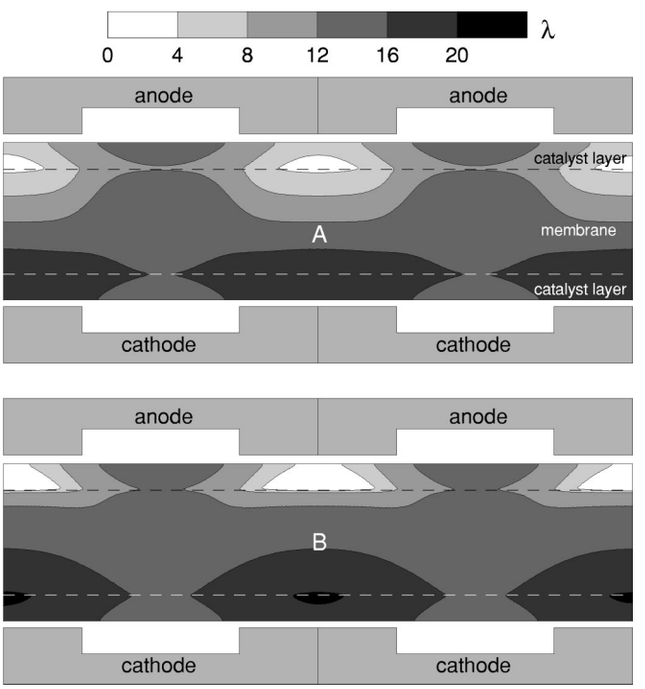

Figure 7. The maps of water content λ in membrane and catalyst layers: (A) with experimental diffusion coefficient D_{wl} (curve A in Fig. 2b), (B) with model D_{wl} (curve B in Fig. 2b). (— — —) The membrane/catalyst layer interfaces. Mean current density in both cases is 0.65 A cm^{-2}. To represent the details the aspect ratio of this figure is distorted, actual ratio of its horizontal to vertical size is about 15.

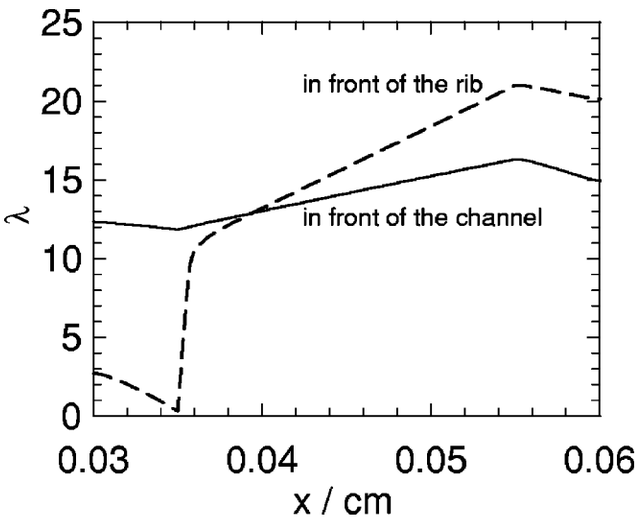

Figure 8. The profiles of water content across the MEA in the first element for model D_{wl} (curve B in Fig. 2b). In front of the feed channel λ is almost constant, whereas in front of the rib a large gradient of λ near the anode forms. Mean current density is 0.65 A cm^{-2}.

The model of Eikerling *et al.*[29] considers the membrane as a porous structure with variable mean pore radius, which depends on water content. According to Ref. 29, water in pores exist in gas and liquid form and pressure difference between the two phases is equal to the capillary pressure. Under constant gas pressure the flux of liquid water in the membrane is driven by the gradient of "liquid" pressure p^l. Pressure p^l then depends solely on mean pore radius, or, inversely, membrane structure depends on p^l.

The central role in the Ref. 29 model plays hydraulic permeability of the membrane, which is taken to be decreasing with water content. Mentioned in Ref. 21, qualitative agreement of measured profile $\overline{\lambda}(x)$ with those calculated by the theory[29] is explained by this successful choice of hydraulic permeability. It was shown above that the diffusion coefficient, which decreases with λ, also provides a qualitatively correct profile $\overline{\lambda}(x)$.

Acknowledgments

The author is grateful to Dr. F. Büchi for the full set of experimental data. The simulations were performed on a Cray T3E computer of the Institute of Applied Mathematics, Research Center "Jülich", Germany.

The Research Center Julich assisted in meeting the publication costs of this article.

Appendix

Transport Coefficients of Water in Membrane

In our model the membrane is characterized by diffusion coefficient D_{wl}, drag coefficient n^d, proton conductivity σ, and the water uptake isotherm Λ.

The literature data on drag coefficient are contradictory. In the range $\lambda > 10$ measurements of Ise *et al.*[30] as well as those of Ren and Gottesfeld[31] give linear growth of n^d with water content. (At $\lambda = 22$ the data of Zawodzinski *et al.*[32] and Xie and Okada[33] agree well with the data of Ise *et al.*[30]). Physically, this growth is explained by the growth of the mean pore radius in the membrane.[30] In larger pores the role of electrostatic "friction" near walls is lower and a large amount of bulk water facilitates drag.

However, at low water content ($\lambda < 10$) the situation is more complicated. Fuller and Newman,[34] Zawodzinski *et al.*,[35] and van Bussel *et al.*[13] reported a constant value of n^d in the range $5 < \lambda < 10$, but below $\lambda = 5$ drag coefficient from Fuller and Newman drops down to zero, whereas n^d from Zawodzinski *et al.* and from van Bussel *et al.* remains constant. In general, the dependence of drag coefficient on λ in this range is still not quite clear; some qualitative considerations are given in Ref. 30.

Springer *et al.*[1] presented measurements of diffusion coefficient D_{wl} for Nafion 117. Corrected for membrane swelling, D_{wl} appeared to be constant in the range $\lambda = 5$. Below $\lambda = 5$ D_{wl} exhibits a distinct peak. This peak can be induced by the procedure of correction[1] which involves differentiation of experimental data.

Recent measurements have shown that D_{wl} drops down with water content.[36,13] *In situ* measurements in the working fuel cell[13] gave almost constant D_{wl} in the range $10 < \lambda < 22$ and drop to zero for $\lambda < 5$. Physically, low water content means lower mean pore radius in the membrane, which presumably hinders water diffusion.

The data of Ref. 13 are shown in Fig. 2 along with the fits, convenient for simulations

$$D_{wl} = 4.1 \times 10^{-6}\left(\frac{\lambda}{25}\right)^{0.15}\left[1 + \tanh\left(\frac{\lambda - 2.5}{1.4}\right)\right], \quad \text{cm}^2\ \text{s}^{-1} \qquad \text{[A-1]}$$

$$n^d = \begin{cases} 1, & \lambda < 9 \\ 0.117 - 0.0544, & \lambda \geqslant 9 \end{cases} \qquad \text{[A-2]}$$

$$\sigma = \begin{cases} 0, & \lambda < 1.253 \\ (0.5738\lambda - 0.7192, & \lambda \geqslant 1.253 \quad \Omega^{-1}\text{cm}^{-1} \end{cases} \qquad \text{[A-3]}$$

Note that all the simulations were performed with constant $n^d = 1$.

The water uptake isotherm $\Lambda(a)$ for the membrane, equilibrated with water vapor at 80°C, was measured in Ref. 23 in the range $0 \leqslant a \leqslant 1$, where $a = c_w/c_w^{sat} = p_w/p_w^{sat}$ is water vapor activity, and $p_w^{sat}(T)$ is water saturation pressure.[1] In our model $\Lambda(a)$ was extrapolated to $a = 3$, as shown in Fig. 1. The fit used is given by

$$\Lambda = 0.3 + 6a[1 - \tanh(a - 0.5)] + 3.9\sqrt{a}\left[1 + \tanh\left(\frac{a - 0.89}{0.23}\right)\right]$$

List of Symbols

c_w	water vapor molar concentration, mol cm^{-3}
c_w^{sat}	molar concentration of saturated water vapor, mol cm^{-3}
c_{wl}	liquid water molar concentration in membrane, mol cm^{-3}
c_{H^+}	molar concentration of protons in membrane
d	thickness of membrane and catalyst layers (Fig. 4), cm
D_w	diffusion coefficient of equivalent water vapor in membrane phase of the catalyst layer, cm^2 s^{-1}
D_{wl}	diffusion coefficient of liquid water in membrane, cm^2 s^{-1}
D_w^b	binary diffusion coefficient of water in backing layer, cm^2 s^{-1}
D_w^K	Knudsen diffusion coefficient of water in catalyst layer, cm^2 s^{-1}
E	electric field strength, V cm^{-1}
F	Faraday constant, 9.6495 × 10^4 Couloumb g mol^{-1}
I	total current, produced by a cell, A
j	local proton current density, A cm^{-2}
$\overline{j}$	mean current density in a cell, A cm^{-2}
H	the width of cell element (Fig. 4), cm
n	number of electrons, participating in reaction
n^d	drag coefficient, a number of water molecules transported by single proton
N	molar flux, mol cm^{-2} s^{-1}
P	membrane volume, cm^3
Q	rate of electrochemical reaction, A cm^{-3}
R_g	gas constant, 8.314 J K^{-1} g mol^{-1}
R	membrane resistance, Ω cm^2
S	stoichiometry factor
T	temperature, K
δV	voltage loss in membrane, V
W	weighing function, cm^{-1}
x	coordinate across the cell, cm
y	coordinate along the cell surface, cm

Subscripts and Superscripts

a	at the anode
b	in the backing layer
c	at the cathode
w	water vapor
wl	liquid water

Greek

- ε membrane fraction in the catalyst layer
- Λ water sorption isotherm
- λ membrane water content, number of water molecules per SO_3 group
- σ electrolyte (membrane phase) conductivity
- φ potential of membrane phase, V

References

1. T. E. Springer, T. A. Zawodzinski, and S. Gottesfeld, *J. Electrochem. Soc.*, **138**, 2334 (1991).
2. D. M. Bernardi and M. W. Verbrugge, *J. Electrochem. Soc.*, **139**, 2477 (1992).
3. G. Murgia, L. Pisani, M. Valentini, and B. D'Aguanno, *J. Electrochem. Soc.*, **149**, A31 (2002).
4. L. Pisani, G. Murgia, M. Valentini, and B. D'Aguanno, *J. Electrochem. Soc.*, **149**, A898 (2002).
5. T. F. Fuller and J. Newman, *J. Electrochem. Soc.*, **140**, 1218 (1993).
6. P. Futerko and I.-M. Hsing, *Electrochim. Acta*, **45**, 1741 (2000).
7. I.-M. Hsing and P. Futerko, *Chem. Eng. Sci.*, **55**, 4209 (2000).
8. S. Um, C.-Y. Wang, and K. S. Chen, *J. Electrochem. Soc.*, **147**, 4485 (2000).
9. T. V. Nguyen and R. E. White, *J. Electrochem. Soc.*, **140**, 2178 (1993).
10. J. S. Yi and T. V. Nguyen, *J. Electrochem. Soc.*, **145**, 1149 (1998).
11. D. Thirumalai and R. E. White, *J. Electrochem. Soc.*, **144**, 1717 (1997).
12. K. Dannenberg, P. Ekdunge, and G. Lindbergh, *J. Appl. Electrochem.*, **30**, 1377 (2000).
13. H. P. L. H. van Bussel, F. G. H. Koene, and R. K. A. M. Mallant, *J. Power Sources*, **71**, 218 (1998).
14. D. Natarajan and T. V. Nguyen, *J. Electrochem. Soc.*, **148**, A1324 (2001).
15. S. Dutta, S. Shimpalee, and J. W. Van Zee, *J. Appl. Electrochem.*, **30**, 135 (2000).
16. S. Shimpalee and S. Dutta, *J. Electrochem. Soc.*, **150**, A341 (2003).
17. A. A. Kulikovsky, J. Divisek, and A. A. Kornyshev, *J. Electrochem. Soc.*, **147**, 953 (2000).
18. A. A. Kulikovsky, *Fuel Cells*, **1**, 162 (2001).
19. G. J. M. Janssen, *J. Electrochem. Soc.*, **148**, A1313 (2001).
20. F. Büchi and G. G. Scherer, *J. Electroanal. Chem.*, **404**, 37 (1996).
21. F. Büchi and G. G. Scherer, *J. Electrochem. Soc.*, **148**, A183 (2001).
22. S. Gottesfeld and T. A. Zawodzinski, in *Advances in Electrochemical Science and Engineering*, Vol. 5, R. C. Alkire, H. Gerischer, D. M. Kolb, and Ch. W. Tobias, Editors, pp. 195-301, Wiley-VCH, Weinheim (1997).
23. J. T. Hinatsu, M. Mizuhata, and H. Takenaka, *J. Electrochem. Soc.*, **141**, 1493 (1994).
24. R. B. Bird, W. E. Stewart, and E. N. Lightfoot, *Transport Phenomena*, Wiley, New York (1960).
25. A. A. Kulikovsky, J. Divisek, and A. A. Kornyshev, *J. Electrochem. Soc.*, **146**, 3981 (1999).
26. J. M. Stockie, K. Promislow, and B. R. Wetton, *Int. J. Numer. Methods Fluids*, **41**, 577 (2003).
27. N. Sato, *J. Phys. D*, **13**, L3 (1980).
28. A. A. Kulikovsky, *J. Comput. Phys.*, **173**, 716 (2001).
29. M. Eikerling, Yu. I. Kharkats, A. A. Kornyshev, and Yu. M. Volfkovich, *J. Electrochem. Soc.*, **145**, 2684 (1998).
30. M. Ise, K. D. Kreuer, and J. Maier, *Solid State Ionics*, **125**, 213 (1999).
31. X. Ren and S. Gottesfeld, *J. Electrochem. Soc.*, **148**, A87 (2001).
32. Th. A. Zawodzinski, Jr, C. Derouin, S. Radzinski, R. J. Sherman, V. T. Smith, Th. E. Springer, and S. Gottefeld, *J. Electrochem. Soc.*, **140**, 1041 (1993).
33. G. Xie and T. Okada, *J. Electrochem. Soc.*, **142**, 3057 (1995).
34. T. F. Fuller and J. Newman, *J. Electrochem. Soc.*, **139**, 1332 (1992).
35. T. A. Zawodzinski, J. Davey, J. Valerio, and S. Gottesfeld, *Electrochim. Acta*, **40**, 297 (1995).
36. K. D. Kreuer, *J. Membr. Sci.*, **185**, 29 (2001).